Winds at the Mars 2020 landing site. Part 2: Wind variability and turbulence

D. Viúdez-Moreiras[1,*], M. de la Torre[2], J. Gómez-Elvira[3], R. D. Lorenz[4], V. Apéstigue[3], S. Guzewich[5], M. Mischna[2], K. Herkenhoff[6], D. Toledo[3], M. Lemmon[7], M. Smith[5], C.E. Newman[8], A. Sánchez-Lavega[9], J.A. Rodríguez-Manfredi[1], R. Hueso[9], A.M. Harri[10], L. Tamppari[2], R. Sullivan[11], I. Arruego[3], J. Bell[12]

[1]Centro de Astrobiología (CSIC-INTA) & National Institute for Aerospace Technology (INTA), Torrejón de Ardoz, Madrid, Spain (viudezmd@inta.es)
[2] Jet Propulsion Laboratory, California Institute of Technology, 4800 Oak Grove Drive, Pasadena, CA 91109, USA.
[3] National Institute for Aerospace Technology (INTA), Torrejón de Ardoz, Madrid, Spain
[4] Johns Hopkins Applied Physics Lab, Laurel, MD, USA.
[5] NASA Goddard Spaceflight Center, Greenbelt, MD, USA.
[6] USGS Astrogeology Science Center, Flagstaff, AZ 86001, USA.
[7] Space Science Institute, College Station, TX 77843 USA.
[8] Aeolis Research, Chandler, AZ, USA.
[9] Universidad del País Vasco (UPV/EHU), Bilbao, Spain
[10] Finnish Meteorological Institute, Helsinki, Finland.
[11] Cornell University, Ithaca, NY, USA
[12] School of Earth and Space Exploration, Arizona State University, Tempe, AZ 85281, USA.

ABSTRACT

This is the second part of a two-part paper. Wind speeds measured by the Mars 2020 Perseverance rover in Jezero crater were fitted as a Weibull distribution. InSight wind data acquired in Elysium Planitia were also used to contextualize observations. Jezero winds were found to be much calmer than in previous missions, despite the intense aeolian activity observed. A great influence of turbulence and wave activity was observed in the wind speed variations, thus driving the probability of reaching the highest wind speeds at Jezero, instead of sustained winds driven by local, regional or large-scale circulation. The power spectral density of wind speed fluctuations follows a power-law, whose slope deviates depending on the time of day from that predicted considering homogeneous and isotropic turbulence. Daytime wave activity may be related to convection cells and smaller eddies in the boundary layer, advected over the crater. The signature of convection cells was also found during dust storm conditions, when winds were likely tide-driven instead of slope-driven. Nighttime fluctuations were also intense, suggesting strong mechanical turbulence. Convective vortices were usually involved in rapid wind fluctuations, and Weibull models were constructed in the periods around their pressure drops, showing extreme winds and relative variations between 0.8 and 9.2 times the background winds. We report the detection of a strong dust cloud of 0.5-1 km passing over the rover. The observed aeolian activity had major implications for instrumentation, with the wind sensor suffering damage throughout the mission, probably due to flying debris advected by winds.

PLAIN LANGUAGE SUMMARY

This is the second part of a two-part paper. Wind speeds measured by Mars 2020 in Jezero crater were fitted as a Weibull probability distribution. InSight wind data acquired in Elysium Planitia were also used to contextualize the observations. Jezero winds were found to be much calmer than in previous missions, despite the intense aeolian activity observed at Jezero crater. A great influence of turbulence was observed in the wind speed variations, thus driving the probability of reaching the highest wind speeds at Jezero, instead of sustained winds. Turbulence and wave activity provoked rapid fluctuations that changed wind speed from calm conditions to more than 10 - 15 ms^{-1} in the timescale of seconds to minutes. Daytime wave activity may be related to convection cells and smaller eddies in the boundary layer, advected over the crater. These convection cells are produced under strong thermal gradients typically present during daytime. Pressure drops, associated with convective vortices, were usually involved in rapid wind fluctuations. We report the detection of a strong dust cloud of 0.5-1 km passing over the rover. The aeolian activity had major implications for instrumentation, with the wind sensor suffering damage probably due to flying debris advected by winds.

KEY POINTS:

1. Jezero winds are found to be much calmer on average than in previous missions.
2. Turbulence and convective vortices drive the peak wind speeds observed at Jezero.
3. We report the detection of a dust cloud of 0.5-1 km passing over the rover.

1. INTRODUCTION

Variability in surface winds is a key element in aeolian studies. Two mechanisms dominate the dust lifting on Mars: surface wind stress lifting and convective vortex lifting. Outside convective vortices, dust is lifted when the surface wind stress exceeds a threshold value, and sand particles are then moved by drag forces that bounce along the surface, in a process known as saltation (e.g., Petrosyan et al., 2011). Saltation responds to changes in wind speed on timescales of a second (Kok et al., 2012 and references therein), therefore both instantaneous and sustainable winds could influence this process. Once in the atmosphere, dust can be quickly transported and retained for longer periods (e.g., Wang et al., 2003; 2005; Basu et al., 2004; Kahre et al., 2006; Sánchez-Lavega et al., 2019) before being deposited. Given the strong extinction of solar radiation that this aerosol species produces in the atmosphere, suspended dust drives weather and climate on Mars (e.g., Pollack et al., 1979; Haberle et al., 1993; Wilson & Hamilton, 1996; Kahre et al., 2017; and references therein). The variability in surface winds also affects the dispersion of chemical species in the Martian planetary boundary layer (PBL) (e.g., Spiga & Forget, 2009; Viúdez-Moreiras et al., 2021a). Also, wind variability can also affect surface missions. Wind gusts, or peak wind speeds inside convective vortices, can damage the instrumentation of in situ robotic missions by flying debris (Viúdez-Moreiras et al., 2019b) and may constrain future manned missions to the surface of Mars.

The variability in surface winds can result from various mechanisms affecting different timescales. On short timescales (i.e., less than an hour) the variability of winds in the Martian PBL, and in the surface layer in particular, is dominated, as on Earth, by turbulence and wave activity. Wind turbulence thus refers to as rapid fluctuations in winds, which can be caused by different phenomena. During the daytime, the strong thermal gradients present on the Martian surface generally imply buoyancy-driven turbulence, while turbulence may be much lower and mechanically driven during the nighttime, when the atmosphere is very stable (even presenting an inversion layer close to surface). Wind variations on longer timescales are mainly controlled by mesoscale and synoptic variations.

The companion paper (part 1) presented the wind patterns as measured in the Jezero crater floor by Mars 2020, and analyzed the mechanisms driving atmospheric circulation at Jezero. This second part complements those results, focusing on wind variability as observed by the mission in all timescales from the turbulent to the seasonal scale. This second part is structured as follows: Section 2 describes the models used to characterize the wind variability. Section 3 presents the average wind variability over the mission, and Section 4 the diurnal, sol-to-sol and seasonal variability of wind speed. Section 5 presents the characterization of wind turbulence and Section 6 describes the extreme winds observed by the Mars 2020 mission. Section 7 presents the interaction between winds and surface. Finally, Section 8 presents the conclusions.

2. METHODS: WEIBULL WIND MODELS

The Mars 2020 wind speeds (see the companion paper, part 1) were characterized by fitting the wind data as a Weibull distribution (e.g., Seguro & Lambert, 2000). InSight wind data acquired in Elysium Planitia (at ~4.5°N, 136°E) were also used for comparative purposes. The Weibull distribution is widely used to characterize wind speed probability distributions on Earth and it has been successfully applied to Martian wind data (Lorenz, 1996; Viúdez-Moreiras et al., 2019b; Schorbach & Weiland; 2022); empirical results have also been applied to parameterize unresolved subgrid turbulence in numerical models (e.g., Roback et al., 2022).

This distribution gives a probability density function (PDF):

$$f(v) = (k/c)(v/c)^{k-1}e^{-(v/c)^k} \qquad \text{(Eq. 1)}$$

and a cumulative probability function:

$$F(v) = 1 - e^{-(v/c)^k} \qquad \text{(Eq. 2)}$$

where the scale parameter c relates to the mean wind speed while the shape parameter k controls the shape of the distribution. Weibull best-fit parameters have been computed for the wind dataset, acquired at 1.5 m, using the procedure described in Viúdez-Moreiras et al. (2019b); that is, the model was fitted by maximum likelihood estimation (MLE) after removing calm periods ($v < 0.2$ ms^{-1}). The percentage of wind speeds with such low velocities was less than 0.1% (see the companion paper, part 1). Unlike the common use of Weibull models on Earth on timescales of 10 min to characterize sustainable wind speeds for wind energy studies, we focus this study, as in Viúdez-Moreiras et al. (2019b), on wind variability on the timescale of seconds, given their relationship with aeolian studies and mission risk assessment (e.g., Lorenz, 1996; Sullivan et al., 2020; Charalambous et al., 2021; Roback et al., 2022). Timescales faster than 0.5 Hz are filtered out by the sensor retrieval process. Thus, models have been performed in this study over the 0.25 Hz wind data (4 s timescale). This is well above the frequency cut-off for the MEDA WS retrievals. As Viúdez-Moreiras et al. (2019b) note, the sampling rate may affect the Weibull parameters, given that wind fluctuations may be filtered as the averaging baseline is increased. Results for other sampling rates appropriate for sustained winds are included for comparative purposes.

To illustrate how the wind speeds at the sensor height, z_s, could be predictive of the wind speed that drives saltation near the surface, the characteristic timescale, τ_e, of the turbulent eddies at z_s relevant for saltation need to be computed. Only turbulent eddies with characteristic length $l > z_s$ are assumed to be able to affect the saltation layer. Thus, $\tau_e \sim (z_s^2/\varepsilon)$, where ε is the dissipation rate of turbulence kinetic energy (TKE) in a neutral atmospheric boundary layer that can be approximated by $u_*^3/(k_v\ z_s)$ (Stull, 2012; Comola et al., 2019), u_* is the friction velocity and k_V the Von Kármán constant, typically ~0.4. Considering mean wind speeds of 3.24 ms^{-1} (see the companion paper, Part 1) and assuming a logarithmic profile under neutral conditions, this leads to τ_e of 5.6 s. Thus, the timescale of the Weibull models agrees with the eddies expected to affect the surface. In any case, Weibull parameters were not found to be very sensitive on the timescales of seconds.

As in MSL REMS data (Gómez-Elvira et al., 2012), the acquisition strategy yielded significant asymmetries in the number of available measurements in particular periods of time; therefore, the data have been normalized in size to correct this irregular distribution of data. Three different model sets have been performed in the temporal scale: (i) an average Weibull model considering the full dataset, representing the variability in the total winds; (ii) models distinguishing several diurnal timeslots, representative of the wind regimes and periods observed in the diurnal cycle, and (iii) a comprehensive characterization as a function of time of day and sol period. The diurnal timeslots are (see the companion paper, part 1): (i) morning (DW), from 07:00 to 10:00 LTST, (ii) midday (MD), from 10:00 to 15:00 LTST, (iii) afternoon (DL), from 15:00 to 18:00 LTST, (iv) night-fall (NF), from 18:00 to 21:00 LTST, (v) night (NL-1), from 21:00 to 24:00 LTST, (vi) midnight (NL-2), from 00:00 to 03:00 LTST, and (vii) early morning (EM), from 03:00 to 07:00 LTST. In MSL, significant gaps were present in the data after removing the low-quality wind data as a result of the sensor failure during MSL landing, forcing averaging of multiple sols in the seasonal characterization performed in (iii). Here, both for InSight and Mars 2020, this averaging was not necessary; hence, 5-sol sliding window models could be produced for the first time.

3. AVERAGE WIND SPEED VARIABILY OVER THE MISSION

Fig. 1 shows the best-fit probability density function for the full Mars 2020 MEDA dataset (mission sol ≤ 315) at the Jezero landing site and for the full InSight dataset at Elysium Planitia landing site. The Weibull distribution fits the wind speed data at Jezero using a scale parameter c = 3.57 ms^{-1} and a shape parameter k = 1.49, and the Elysium Planitia using a scale parameter c = 6.20 ms^{-1} and a shape parameter k = 1.92.

These parameters align with those found at Gale Crater (Viúdez-Moreiras et al., 2019b), which were obtained in the same timescale, although Jezero crater winds were much quieter than those found in previous missions. Notably, the results at Gale exclude the period of 3 - 7 LTST (EM timeslot) due to lack of high-quality wind data. With only the exclusion of this timeslot, the same models obtained for Jezero and Elysium Planitia are shown in Table 1 for comparative purposes. Among the three landing sites on Mars in which high-frequency measurements are available, Jezero crater showed the lowest total wind speeds (the wind speeds considering all timeslots throughout the sol) excluding the EM timeslot. This result was reproduced even constraining the dataset to the same seasonal period covered by Mars 2020 (L_s~22º to L_s~155º) in the InSight data (Table 1 and Table 2). It leads to wind speed probabilities P(v > 8 ms^{-1}) of ~21% and 3.6%, respectively, at the Elysium Planitia and Jezero landing sites, and P(v > 12 ms^{-1}) of 5.1% and 0.2%, respectively. At the Elysium Planitia landing site, 95% of wind speeds were below 12.1 ms^{-1} and 99% of wind speeds were below 15.7 ms^{-1}. At the Jezero landing site, 95% of wind speeds were below 7.46 ms^{-1} and 99% of wind speeds were below 9.95 ms^{-1} (Table 2).

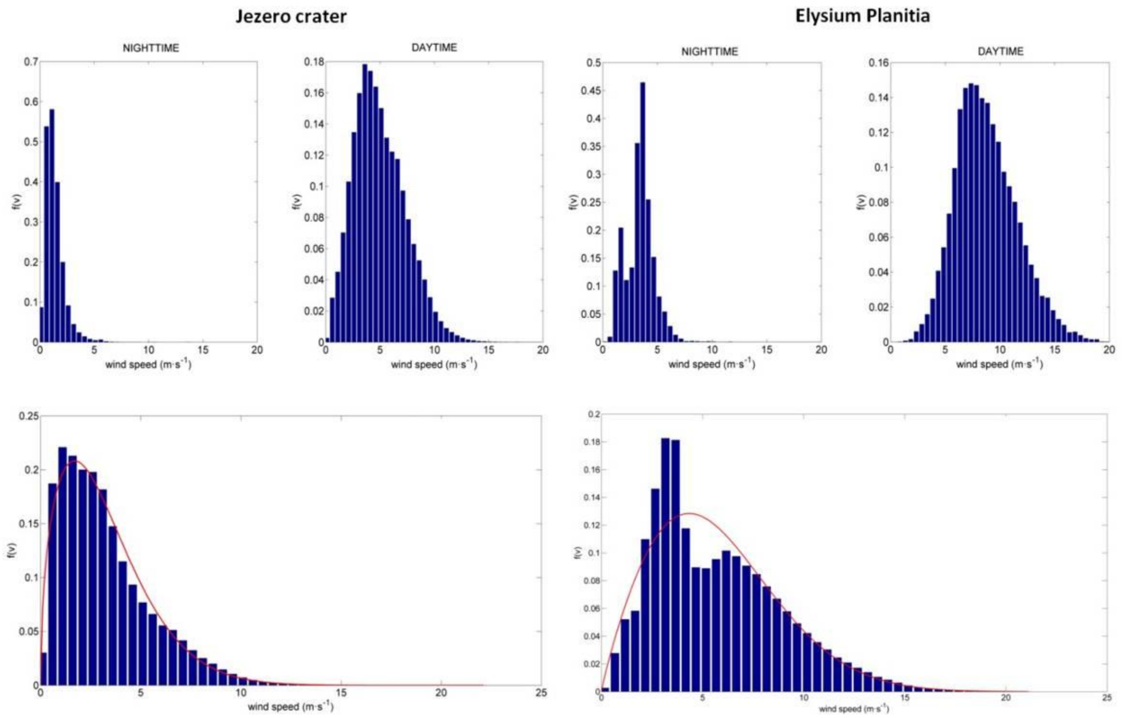

Fig. 1: (**left**) Weibull probability density function obtained for Jezero (red line) and comparison with Mars 2020 MEDA data (blue histogram) for the whole sol and splitting the nighttime (3 – 7 h LTST) and the daytime (10 – 18 h LTST). (**right**) As in the left, but for Elysium Planitia, and comparison with InSight TWINS data. Daytime and nighttime histograms are also shown highlighting the different regimes found in both landing sites.

The wind variability derived from the previously described Weibull parameters involved all the timescales in wind variations, from the faster timescales to the large-scale variations in the seasonal pattern. Ten-minute averages instead of high-frequency measurements, mostly removing the turbulent scales, showed a null difference on the *c* parameters, and an increase in the *k* parameter, from 1.49 to 1.71, leading to P(v > 8 ms^{-1}) and P(v > 12 ms^{-1}) of ~2% and ~0.04%, respectively, thus strongly reducing the probabilities of high wind speeds. This result is indicative of the great influence of sudden changes in wind speed rather than sustained winds driven by mesoscale or large-scale dynamics in the observed wind speed variability, with turbulence driving the likelihood of high wind speeds being reached at Jezero.

The wind speed distributions at Jezero, as well as at Elysium Planitia, presented marked diurnal variation, in accordance with changes in the wind regimes throughout the diurnal cycle (Table 1 and Table 2). At the Jezero landing site, the highest average wind speeds were found in the afternoon (DL timeslot, v = 6.08 ms^{-1} and c = 6.80 ms^{-1}). Wind speeds were also high, on average, during the midday (MD) timeslot (v = 4.67 ms^{-1} and c = 5.28 ms^{-1}). There was a large break with the remaining timeslots, which presented v < 3.1 ms^{-1}

and c < 3.5 ms^{-1}. Wind speed probability P(v > 8 ms^{-1}) equaled ~20% during the afternoon (DL timeslot), and such a probability was negligible (<0.2%) for all the timeslots during the night (NL-1, NL-2 and EM). Also, during the DL timeslot, 99% of wind speeds were below 11.3 ms^{-1}, whilst, during the EM timeslot, 99% of wind speeds were below 2.84 ms^{-1} (Table 2). These results highlight the intensity and convective activity involved in the westerly-northwesterly winds observed during the day.

		Elysium Planitia *		Elysium Planitia **		Jezero crater ***	
Timeslot	LTST range	c (m/s)	k	c (m/s)	k	c (m/s)	k
Morning (DW)	07:00-10:00	8.54	2.91	9.74	3.73	3.02	2.01
Midday (MD)	10:00-15:00	8.87	2.77	10.28	3.60	5.28	2.16
Afternoon (DL)	15:00-18:00	6.26	1.93	6.86	1.90	6.80	3.02
Night fall (NF)	18:00-21:00	3.31	1.97	2.18	2.62	3.24	1.97
Night (NL-1)	21:00-24:00	4.32	2.25	2.94	3.60	3.42	2.54
Night (NL-2)	00:00-03:00	5.12	2.34	3.48	4.04	2.13	1.49
Early mor. (EM)	03:00-07:00	4.88	2.69	4.12	2.66	1.31	1.97
Total except EM	_	6.45	1.89	6.63	1.64	4.19	1.75
Total	_	6.20	1.92	6.13	1.62	3.57	1.49

* InSight full dataset; acquired between MY34 L_s~330º and MY36 L_s~153º

** InSight dataset; acquired at the same season than as the M2020 data (L_s~022º to L_s~153º)

*** M2020 full dataset until the WS failure at sol 315; acquired between MY36 L_s~022º to L_s~153º

Table 1: Weibull best-fit parameters for different times of sol at the Jezero landing site. Comparison with those obtained for Elysium Planitia as measured by InSight lander.

	Elysium Planitia *			Elysium Planitia **			Jezero crater ***		
Timeslot	v (m/s)	F^{-1}(0.95)	F^{-1}(0.99)	v (m/s)	F^{-1}(0.95)	F^{-1}(0.99)	v (m/s)	F^{-1}(0.95)	F^{-1}(0.99)
Morning (DW)	7.64	12.50	14.50	8.80	13.01	14.58	2.68	5.22	6.47
Midday (MD)	7.93	13.26	15.49	9.28	13.87	15.61	4.67	8.77	10.69
Afternoon (DL)	5.53	11.02	13.77	6.10	12.22	15.31	6.08	9.78	11.28
Night fall (NF)	2.92	5.76	7.15	1.93	3.31	3.90	2.87	5.66	7.03
Night (NL-1)	3.80	7.02	8.50	2.64	3.99	4.50	3.04	5.26	6.23
Night (NL-2)	4.53	8.17	9.81	3.16	4.57	5.08	1.91	4.45	5.94
Early mor. (EM)	4.36	7.38	8.66	3.67	6.20	7.27	1.16	2.29	2.84
Total except EM	5.72	11.54	14.49	5.90	12.88	16.72	3.73	7.84	10.01
Total	5.49	11.01	13.78	5.45	12.06	15.73	3.22	7.46	9.95

Table 2: Wind speed statistics at 1.5 m, in ms^{-1} (mean wind speed, v, and $F^{-1}(\alpha)$, i.e. wind speed u such as $P(v \leq u) = \alpha$, both for α=95% and α=99%, related to the Weibull parameters presented in Table 1.

Maximum wind speeds were measured in the DL timeslot, matching the period of strongest regional and local upslope winds acting constructively (see the companion paper, part 1). This timeslot involved very stable wind directions and speeds, without significant departures from mean wind speeds. A high value of *k* largely overcame the characteristic *k* parameter of the Rayleigh distribution. A high *k* parameter value was found as well during NL-1 (21-24 h LTST), where sustainable downslope winds were present, although in that case presenting lower mean wind speeds (see the companion paper, part 1). The lowest *k* parameter was found during the NL-2 period (00-03 h LTST), due to downslope flows lasting various lengths in this timeslot. As described in the companion paper, the first part of the night, from sunset to 01 h LTST, presented quite stable westerly/northwesterly downslope winds, peaking around midnight. After that time, winds decreased in intensity towards a calm period. The strength of the downslope winds at NL-2 also had marked seasonal variation. Thus, the low value in the *k* parameter can be attributed to both periods with very different wind features acting together, and with a marked variability in longer timescales. This was also observed in the parameters related to the total winds at Jezero, considering and excluding the calm period (EM timeslot). The remaining diurnal timeslots/periods presented values close to a Rayleigh distribution.

Surface winds at InSight's landing site were the result of complex interaction between regional and local slope flows induced by Elysium Planitia topography, producing a diurnal perturbation superimposed on a mean flow, dominated by the Hadley cell but with modifications due to channeling effects from the regional topography (Banfield et al., 2020; Viúdez-Moreiras et al., 2020). The seasonal period covered by Mars 2020 wind data (L_s~22º to L_s~153º) was characterized by average southeasterly winds close to the equinoxes, which turned to southerlies around the northern summer solstice due to the enhanced zonal mean southern large-scale circulation. Between L_s~153º and L_s~22º (the period not covered by Mars 2020 wind data), mean surface wind speeds at Elysium Planitia were west-northwesterlies between L_s~200º and 320º due to the effect of northerlies by the zonal mean northern large-scale circulation, including two transition periods at L_s~153º-200º and at L_s~320-153º. Diurnal-mean wind speeds peaked close to the northern winter solstice. Note that little interannual variability was observed in the wind data, except (i) during dust storm periods (e.g., MY34/2019 LDS in northern winter, outside the period covered by Mars 2020 data), and (ii) during MY36, where the sparse data acquired presented lower wind speeds (<10% on average) in particular periods.

Most of the diurnal timeslots (Table 1) at the Elysium Planitia landing site showed both higher average wind speeds and steadiness than at Mars 2020 Perseverance's landing site, evaluating the same seasonal period for both landing sites. This could be the result of a lack of significant topography at InSight's landing site. Wind speeds at Elysium Planitia were 72% greater, on average, than at Jezero, which further increased to more than 200% between 03-10 h LTST (EM and DW timeslots), that is, the calm period observed in Jezero crater at night is a unique feature of the crater (probably due to convergent downslope flows on the crater floor acting destructively), which was not observed in the plains of Elysium Planitia.

InSight's landing site showed the opposite results in terms of the skewness of the Weibull distribution. The most constant winds were found after midnight, between 00 and 03 h LTST, when downslope flows produced a rotation from northwesterlies to southwesterlies, while the most variable winds were found during the afternoon (15-18 h LTST), when the observed wind speeds decreased as upslope winds diminished in strength. This difference highlights the distinct wind distributions obtained at the same diurnal timeslots at both landing sites, each driven by its own mesoscale and large-scale phenomena.

4. DIURNAL, SOL-TO-SOL AND SEASONAL VARIABILITY IN WIND SPEED

To see how the results are affected by seasonality and sol-to-sol variability, it is useful to focus now on these multisol timescales. As stated, sol-to-sol variations could not be performed with MSL as a result of the sparse data available due to the loss of a wind sensor boom (Viúdez-Moreiras et al., 2019a; 2019b), needing averaging over several sol periods (100-sols sliding windows) to evaluate seasonal trends. Mars 2020 data involve significant gaps as well, although to a lesser extent, allowing a 5-sol sliding window. This filtering probably removes a significant portion of the atmospheric travelling waves at Jezero (see the companion paper, part 1). Fig. 2 presents the probabilities of wind speeds greater than 4 ms^{-1} as a function of season for the diurnal timeslots considered in Table 1. The EM timeslot (03:00-07:00 LTST) is excluded due to its low number of $P(v > 4\ ms^{-1})$ values.

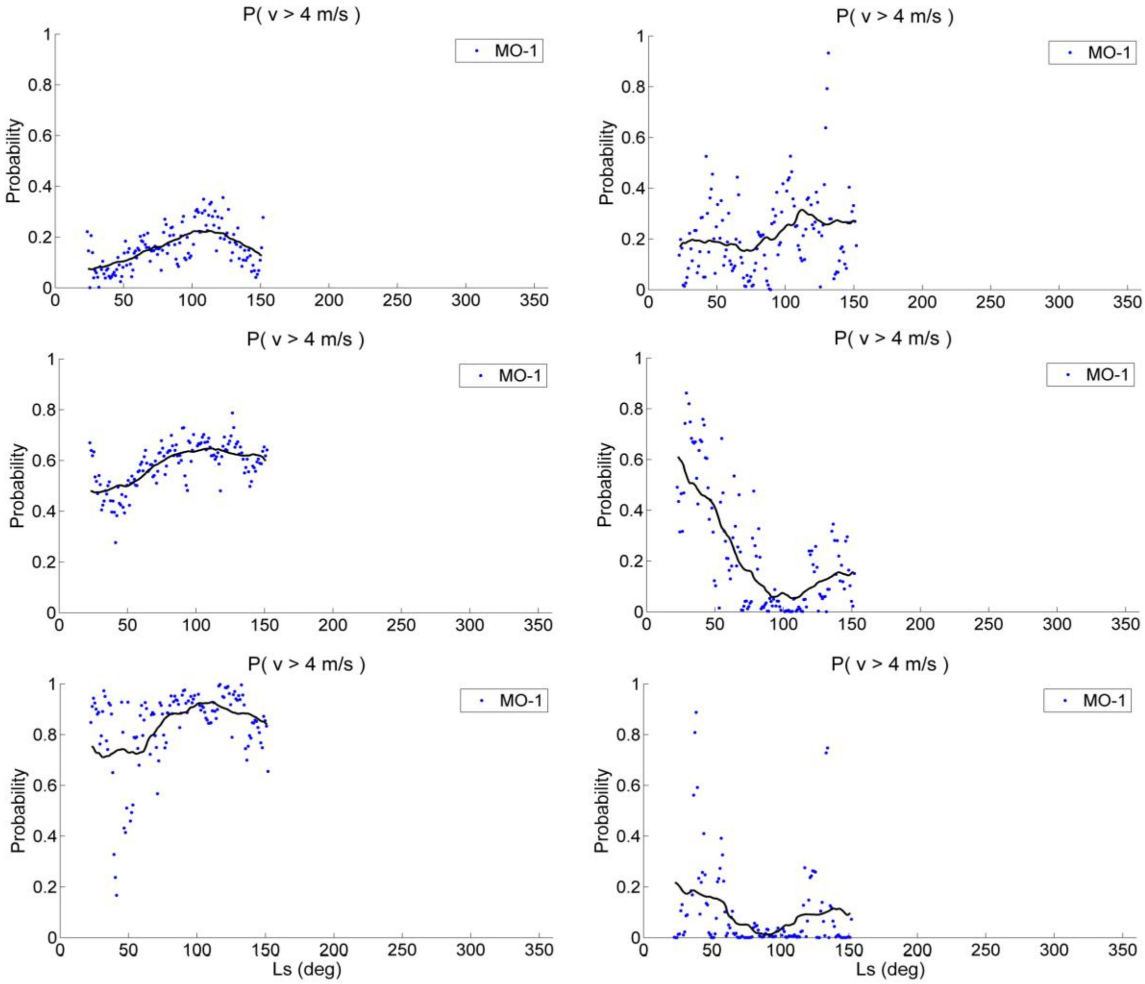

Fig. 2: Seasonal variability in probabilities of wind speeds greater than 4 ms^{-1} for Jezero, based on Weibull models using MEDA wind data for Jezero landing site. From top to bottom: DW, MD, DL (left column) and NF, NL-1 and NL-2 (right column). The EM timeslot (03:00-07:00 LTST) is excluded given the negligible $P(v > 4\ ms^{-1})$ values. A moving average as a function of L_s is also added.

The diurnal trend in $P(v > 4\ ms^{-1})$ (Fig. 2) is consistent with the observed trend in mean wind speeds (see Table 1 and the companion paper). High $P(v > 4\ ms^{-1})$ was observed in the afternoon (DL timeslot), generally greater than 70%, followed by the midday (MD timeslot) with $40\% < P(v > 4\ ms^{-1}) < 70\%$. The daytime timeslots presented a seasonal behavior with maximum values in early summer. The nighttime timeslots showed a huge seasonal variability. At the beginning of the Mars 2020 observations (L_s~22º), $P(v > 4\ ms^{-1})$ at NL-1 (21:00-24:00) reached ~90%. $P(v > 4\ ms^{-1})$ were close to 40% in the first sols of the mission; then, they decreased progressively to less than 10% in early summer and increased again at L_s~150º. A similar trend was observed in NL-2, with $P(v > 4\ ms^{-1})$ close to zero in early summer. This opposite behavior in the seasonal trend between nighttime and daytime was the result of the wind regimes observed at Jezero. Thus, the daytime regime is driven by regional anabatic upslope flows, likely enhanced around the summer solstice by larger thermal gradients and probably affected by Hadley cell return flow (see the companion paper, part 1). Conversely, the nighttime regime (21:00-03:00 LTST) is driven by downslope flows, probably katabatic, which presented strong variability in wind direction as a result of regional and local slope flows competing on the Jezero crater floor and, thus, being very sensitive to variations in rover location. However, together with the results presented in part 1, these observations suggest the possibility of some influence, even during nighttime, from the zonal-mean southerly large-scale flows around the summer solstice, increasing the daytime winds and reducing the intensity of nighttime winds.

Fig. 3 shows the trend for P(v > 8 ms^{-1}) and P(v > 12 ms^{-1}) focusing on the diurnal timeslots where maximum wind speeds were measured (MD and DL timeslots). P(v > 8 ms^{-1}) and P(v > 12 ms^{-1}) never exceed 40% and 10%, respectively. This contrasts with the observations at Gale Crater (Viúdez-Moreiras et al., 2019b) and at Elysium Planitia, where probabilities of high wind speed largely overcome the Jezero values, reaching P(v > 8 ms^{-1}) and P(v > 12 ms^{-1}) of 90% and 45%, respectively. The sol-to-sol variability in the probability of high wind speeds is mostly associated with the stochastic nature of weather, although the effects of atmospheric travelling and gravity waves were also detected (see companion paper, part 1).

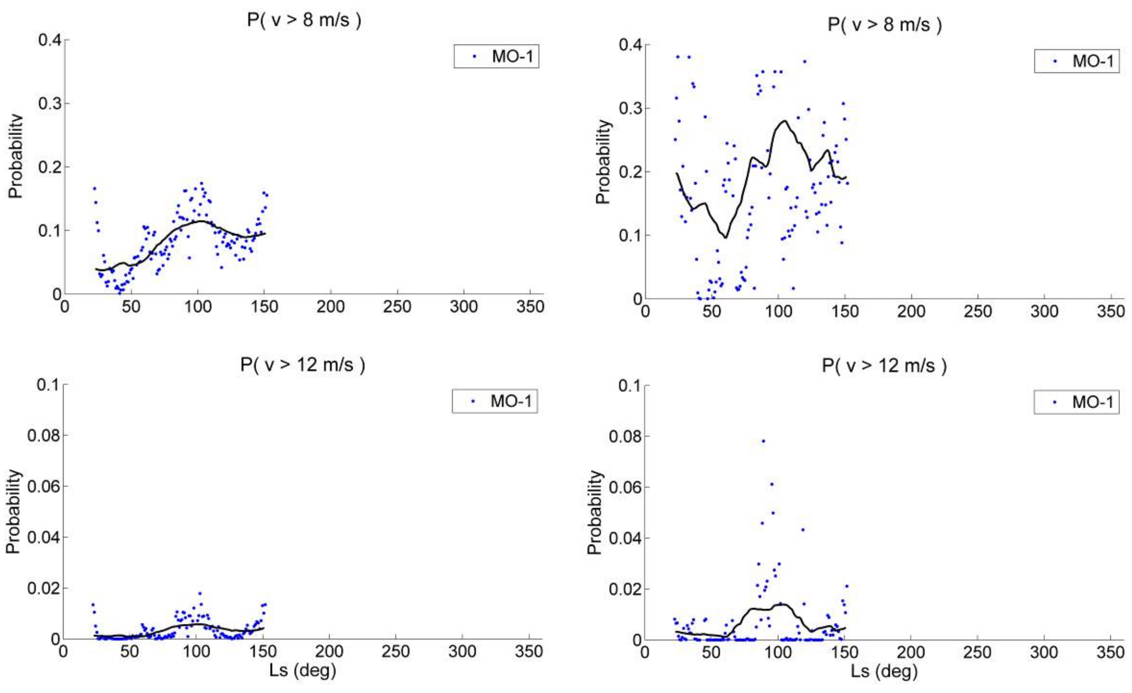

Fig. 3: As in Fig. 2 but for 8 ms^{-1} and 12 ms^{-1} and restricted to the two diurnal timeslots with highest wind speeds, MD (left column) and DL (right column).

5. TURBULENCE AND WAVE ACTIVITY

As described, a significant contribution to the variability in Mars 2020 winds present in the wind speed histograms can be allocated to the sol-to-sol and seasonal timescales. Additionally, the mesoscale and large-scale domains mostly shaped the wind variability in the diurnal timescale. However, most of the variability was produced on turbulent scales. The latter scale is an unexplored area, given the few high-frequency wind measurements from the Martian surface to date.

On Earth, the spectra of surface winds can be divided into three different parts (e.g., Petrosyan et al., 2011): (i) the low-frequency range, where TKE production takes place in the PBL, presenting a slight negative slope or even a constant value, (ii) the inertial subrange, where viscous dissipation is relatively weak and TKE is freely exchanged between length scales, approaching a power law, and (iii) a high frequency range where viscous dissipation becomes relevant and energy drops rapidly. Given that the kinematic viscosity in the near-surface atmosphere of Mars is much greater than on Earth, the Kolmogorov scale of viscous dissipation scales accordingly up to values that may be of the order of centimeters, albeit with time scales that mostly remain above the sampling rate of the wind sensor. Thus, the wind spectra acquired by MEDA could be subscribed mostly to the production range and to the inertial subrange. Fig. 4 shows the power spectral density (PSD) of the wind speed on a typical sol. It can be seen that the slope departs from that predicted by the Kolmogorov model (-5/3) considering homogeneous and isotropic turbulence, approaching the Taylor slope between ~$3\cdot10^{-2}$ and $5\cdot10^{-1}$ Hz (the WS cutoff). The departure follows a diurnal cycle, being higher at night, where the turbulence is mostly mechanically driven.

Thus, periodic wind fluctuations were commonly present in the wind data, but without an overall dominant frequency, either during the day or at night. However, certain daytime timeslot periods presented a dominant oscillation frequency in the wind fluctuations, which in some cases matched with oscillations in other meteorological variables such as with atmospheric pressure. These cases usually appeared during short periods of time. Fig. 5 presents some examples of the time evolution of winds obtained by Mars 2020 MEDA during the daytime. Wind turbulence and wave activity overwhelmed the signal, provoking rapid fluctuations that changed wind speed from calm conditions to more than 10 - 15 ms^{-1} on short timescales. These fluctuations were also present in wind directions. Pressure drops, associated with convective vortices, were usually involved in rapid wind fluctuations and tended to elevate wind speeds in accordance with what was expected by model predictions (Balme et al., 2012; Lorenz, 2016; Kahanpää & Viúdez-Moreiras, 2021). Fig. 5b shows high-frequency wind oscillations on sol 269, mostly dominant between 11.75 h and 11.80 h LTST, with a ~1.5 min period. Fig. 5a and 5c (sols 222 and 313, respectively) show relatively rare cases where oscillations, coupled with surface wind gusts, were sustainable in time and presented a remarkable period of oscillation (~15 - 20 min for sol 222 and ~2 – 3 min for sol 313), with background winds roughly in 5 ms^{-1} in both cases.

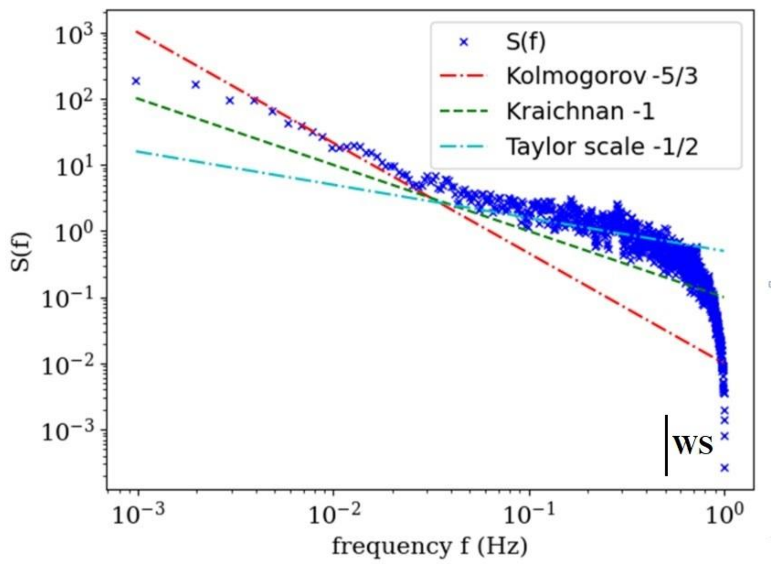

Fig. 4: Power spectral density (PSD, m^2s^{-2} Hz^{-1}) for the fluctuations in wind speed over a set of 3 sols (116-118), defined as a difference to their 720 s running means. Some models are shown for comparative purposes. The region highlighted as WS is affected by WS sampling (see text). The vertical line at 0.5 Hz shows the cutoff of the wind data.

These periodic wind fluctuations, which occur during the convective period, may be related to convection cells and smaller eddies in the PBL advected over the crater at different scales. Convection cells are supported by mesoscale models and large eddy simulations (Spiga et al., 2021; Newman et al.; 2022). Newman et al. (2022) suggested convection cells with periodicities of 8.6 - 15 min (cell widths from 2.4 km to 5.3 km), based on analysis of wind fluctuations on sols 116 – 120. Spiga et al. (2021) reported, based on the InSight dataset, fluctuations in agreement with convection cells advected over Elysium Planitia with periods from 16 to 33 min, suggesting cell widths from 10.5 km to 16 km. Lorenz et al. (2021) found ~10-min wind fluctuations likely produced by convection cells in correlation with temperature variations in the InSight solar arrays. Quasiperiodic wind fluctuations can also be observed in the high-frequency wind data from the Viking Landers (Lorenz et al., 2017). The cases showed here using Mars 2020 wind data, in which particular periodic signals greatly overwhelmed other harmonics (e.g., sol 222, 269 and 313), would suggest length scales between 4 km – 6 km, 400 m – 500 m and 700 m to 1.2 km, respectively. Note that the latter sol corresponds to dust storm conditions, in which winds are believed to be tidally driven instead of slope driven (see the companion paper, part 1).

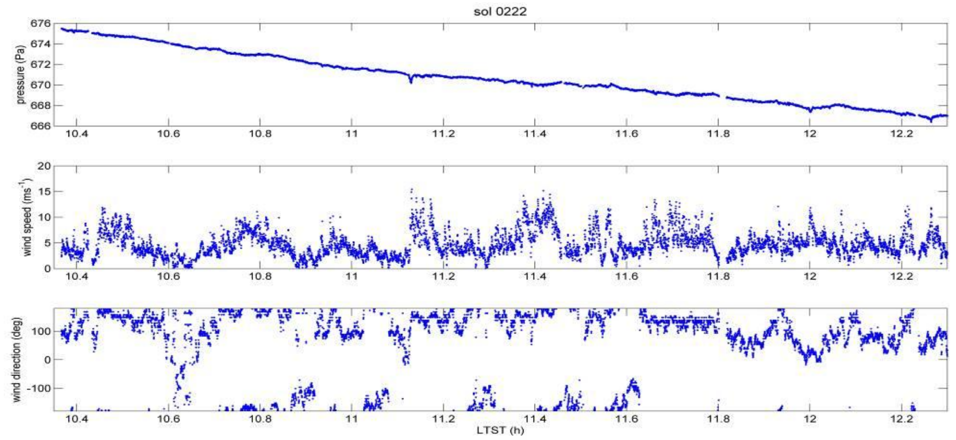

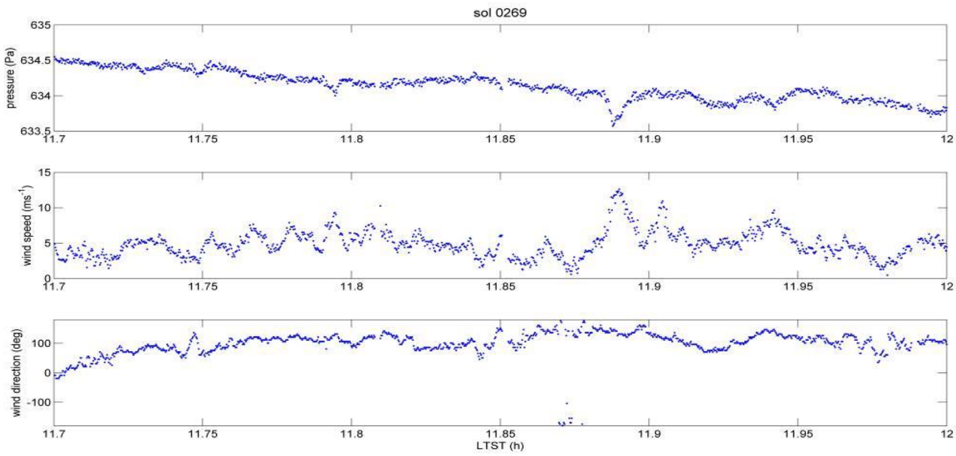

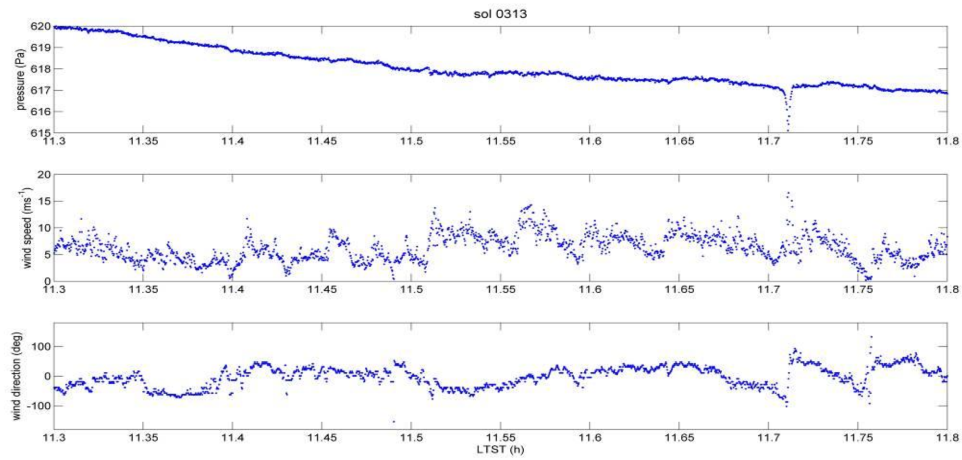

Fig. 5: Evolution in time of high-frequency measurements for three mission sols (222, 269 and 313). Pressure, wind speed and direction are shown for each sol. Regular wind oscillations can be observed during these periods.

The wave period of those fluctuations varied one order of magnitude from the timescale of 1 min - 10 min, while background wind speeds were roughly similar. This would lead to length scales from a few hundred of meters to 6 km, indicative of the turbulent activity present in the daytime Martian PBL. It has been suggested that the Martian PBL depth could be inferred based on the estimated width of convection cells, hence providing valuable information about the PBL. However, these results suggest that is questionable to infer the PBL depth from periodic waves in wind signals, which will likely not relate with the wider length scale of the convection cell, leading to significant underestimations of the PBL depth.

Although the highest intensity in wind fluctuations was observed during the daytime, nighttime variability was also strong. Fig. 6 shows the diurnal cycle for wind fluctuations both represented as standard deviation of wind speed (σ_v) and as turbulence intensity (TI), the last one computed as the standard deviation of wind speeds, σ_v, divided by their mean *v* in periods of 10 min. As the rover elements and the radioisotope thermoelectric generator (RTG) thermal plume can perturb the flow towards the sensors (Fig. 7), the rear flows were not considered to compute σ_v and TI (see the companion paper, part 1). Clearly, fluctuations dominated overall during daytime in both variables, although to a lesser extent once standard deviation is normalized to the mean wind speed. The wind fluctuations were mostly driven by turbulence given the timescale of the averaging (10 min), with a significant contribution of wave activity during daytime. For that period, convection dominates in the statically unstable Martian PBL; hence, turbulence is primarily buoyancy-driven. During nighttime, however, a stable inversion layer is typically produced (e.g., Mason & Smith, 2021), buoyancy-driven turbulence is mostly suppressed and shear-driven turbulence usually dominates. During dust storm periods, the static stability in the nighttime PBL lessens, and the inversion layer may even be absent during long sol periods, as was observed during the MY34/2019 global dust storm (Viúdez-Moreiras et al., 2019c).

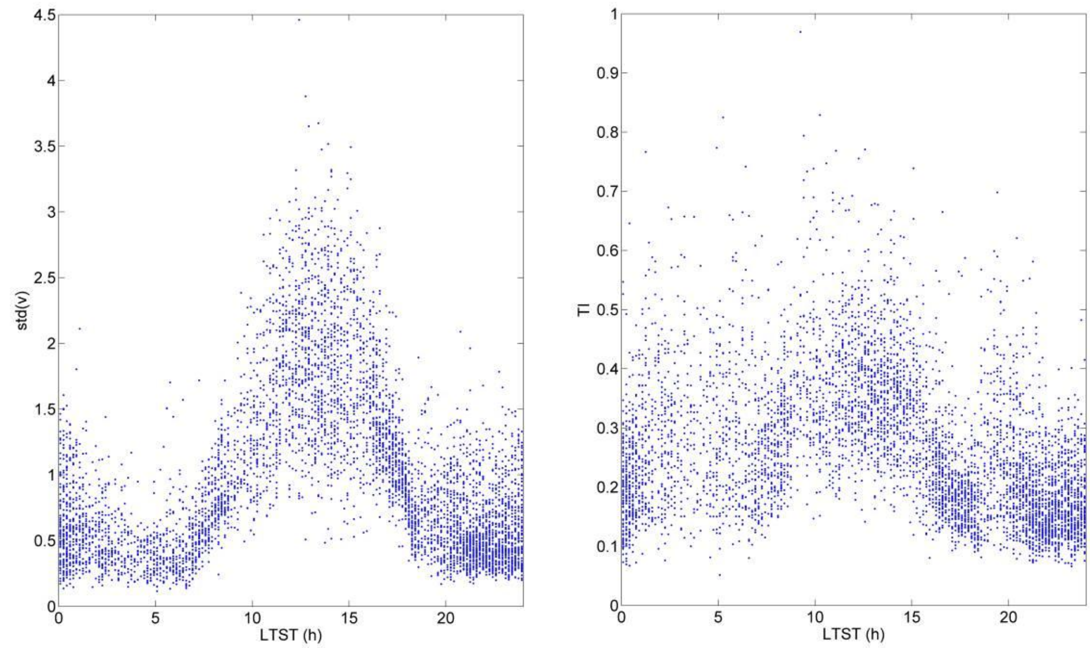

Fig. 6: Diurnal cycle of wind fluctuations as observed by Mars 2020. (**left**) Standard deviation of wind speed; (**right**) Turbulence intensity (TI), defined as standard deviation of wind speed, σ_v, in a 10-min period divided by the mean wind speed v.

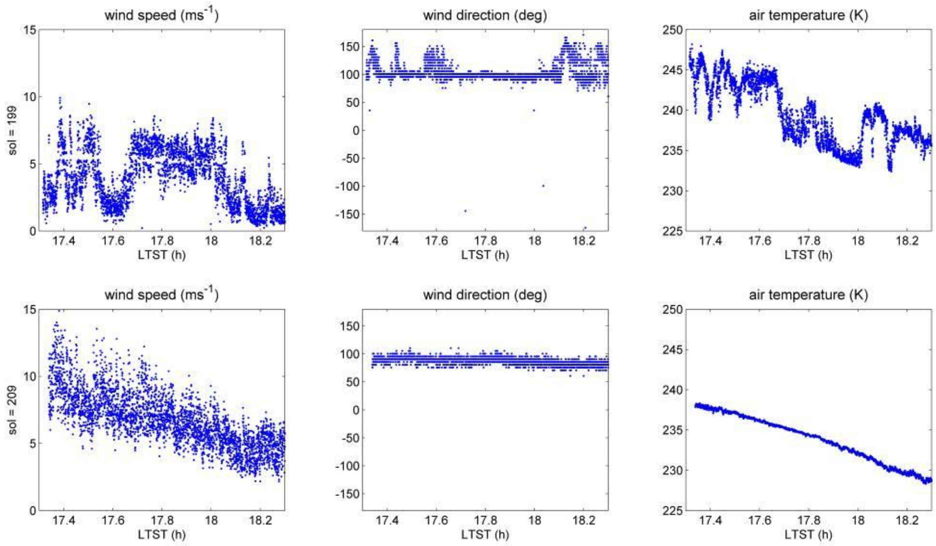

Fig. 7: Effect of the RTG plume disturbance in the wind measurements when winds come from the rear of the rover. Wind speed, wind direction and air temperature are shown in the left, mid and right columns respectively, for the same diurnal timeslot and at two different sols, sol 199 (top row, presenting high RTG contamination due to rear incoming flow) and sol 209 (bottom row, without remarkable RTG contamination with front incoming flow).

Mars 2020 wind data presented in Fig. 6 shows σ_v of 0.57±0.29 ms^{-1} during nighttime and 1.85±0.57 ms^{-1} during the daytime, with peak values greater than ~3.5 ms^{-1} around midday, when thermal gradients are at their maximum. They slightly shifted to the afternoon, due to the dependence of wind fluctuations with wind speed. Turbulence intensity was 36±10% during the day. However, it is interesting to note the dip in the wind fluctuations during the daytime period where sustainable winds peaked, i.e., during the late afternoon (~17 h LTST, see the companion paper, part 1). TI at that time was comparable in magnitude with the nighttime. After sunset, a dramatic increase in TI could be observed at 19 – 21 h LTST, which related to the transition between upslope flows to downslope flows, provoking a full rotation of winds around this period and, in some cases, a burst in wind speeds (see the companion paper, part 1). Nighttime wind fluctuations were also strong, 22% ±10%, and comparable to the daytime TI in some cases, which suggests strong mechanical (shear) turbulence during that period.

Previous missions reported σ_v/v, in particular periods on Mars, which may deviate from the TI values reported in Fig. 6 due to differences in the sampling rate and averaging of wind data. Phoenix data showed σ_v/v values around the local summer solstice between 15% and 40% during the daytime and 4% during the nighttime, as calculated from 32 image exposures as a function of LMST (Holstein et al., 2010). InSight data showed daytime σ_v/v values varying from 35% to 45% at the northern spring equinox to values below 25 – 30% at the summer solstice, using 3 h (11 – 14 h) as the basis of the computation (Spiga et al., 2021). Analysis of the first sols of the Viking Lander missions suggested σ_v/v ~50% – 60%, with more complex variations in diurnal behavior than those observed in the rest of the missions, and both daytime and nighttime local maxima, σ_v/v peaking at ~85% (Murdoch et al., 2017). However, the different data processing from each mission prevents a proper comparison between them. We have computed the TI from InSight data using the same procedure as in Fig. 6 for Mars 2020 data, retrieving TI ~29% ±7% during the day and TI ~12% ±5% during the night. Thus, the TI levels detected by Mars 2020 at Jezero are greater than those detected by InSight at Elysium Planitia, and both produced by buoyancy and shear-driven turbulence.

6. EXTREME WINDS

Extreme winds are generally involved on short timescales in the form of wind gusts produced by turbulent activity, such as the passage of convective vortices. Therefore, high-frequency data are necessary to properly detect them. The timescales in which these gusts emerge can even be less than a few seconds, so the typical 1 Hz sampling rate (or 2 Hz at the beginning of the mission) could be suppressing or biasing the maximum wind speeds in some events, even omitting some of them as a whole. In any case, several events showing extreme winds have been observed in the wind data, and most were associated with the passage of convective vortices.

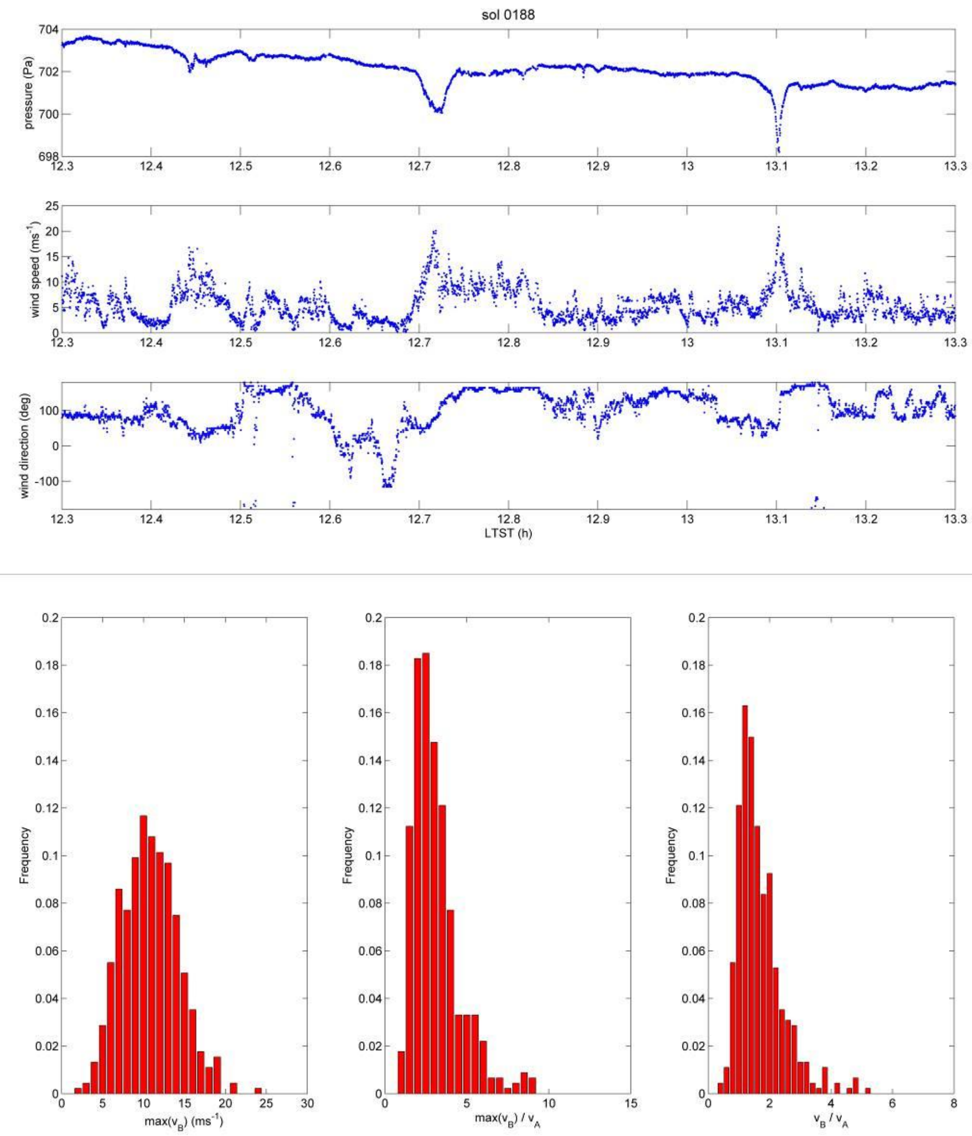

Fig. 8: (**top**) As in Fig. 5 but for sol 188, showing the extreme winds produced during the passage of convective vortices as observed by the Perseverance rover. Pressure, wind speed and direction are shown. (**bottom**) Histograms for wind speeds reached in pressure drops events: (**bottom-left**) peak wind speed reached during the passage, (**bottom-midle**) as in left but normalized to the mean wind speed just before the events, (**bottom-right**) ratio between the mean wind speeds in the event and just before the event.

Fig. 8 shows the passage of three vortices with very different geometries close to the rover in a timescale of an hour (at 12.45 h, 12,72 h and 13.1 h LTST). All three produced a dramatic increase in wind speed and a remarkable effect on wind direction, in addition to a remarkable pressure drop, commonly associated with these events. As stated, the effect on vortex winds on a stationary observer will depend on the geometry of the pass and on the vortex characteristics. In most cases, however, the net effect during the event is an overall increase in wind speeds (e.g., Kahanpää & Viúdez-Moreiras, 2021). Fig. 8 presents, at the bottom, the histogram of peak wind speeds reached during the detected pressure drop events with available wind data (more than 400 events) as observed by Perseverance, in addition to histograms showing the normalized values to the mean wind speed just before the events, and the ratio between the mean wind speeds during the event and just before it. The wind speed signal is treated with a low-pass 4 s filter to minimize random uncertainties and to produce comparable results with the Weibull models presented in the previous section. The peak wind speeds are therefore derived on this timescale. Peak wind speeds observed during these events at the Perseverance location ranged between 2 ms^{-1} and 24 ms^{-1}, with an average of 10.8 ms^{-1}, meaning relative variations between 0.8 and 9.2 times the background winds. The mean wind speeds normalized to the background winds increased on average 1.7, ranging between 0.4 and 5.1. These results emphasize the dramatic effect these events have on the near-surface wind field.

Due to the rarity of these events, Weibull models presented in the previous sections are mostly insensitive to the high wind speeds developed during most of passages. Thus, additional Weibull models were constructed in the periods around the pressure drops detected throughout the mission, as well as when wind data were available. Observations at Jezero crater led to a similar number of pressure drops and intensity as those observed at Elysium Planitia (Spiga et al., 2021; Newman et al., 2022; Hueso et al., this issue). The pressure drop detection algorithm used in this study follows the same principles as those used in previous studies and, thus, retrieves similar results on the distribution of pressure drops associated to convective vortices within the diurnal cycle, with maximum values observed around midday (MD timeslot), when peak thermal gradients occur in the daytime PBL. Weibull models for the MD diurnal timeslot are shown in Fig. 9, both for the whole timeslot period and constraining the analysis to the periods where pressure drop events were observed. The scale parameter c increases 65% and the shape parameter k increases slightly, from 2.16 to 2.36. This variation in the Weibull parameters results in a dramatic effect in the tail of the PDFs at Jezero and, consequently, in the probability of high wind speeds. Thus, $P(v > 8\ ms^{-1})$ increased from 8.6% to 44% and $P(v > 12\ ms^{-1})$ further increased roughly 40 times inside the periods of these events. Curiously, the effect was not as pronounced in the InSight data. The c parameter increased only 12% and the k parameter decreased from 2.77 to 2.55. In any case, the probabilities of high wind speeds rose: for example, P(v > 12 ms^{-1}) increased from 10% to 20%. This difference between the two missions could be influenced by the wind sensor employed on Mars 2020, which is more advanced and allows higher accuracy and better response time than its predecessors, which may affect the instrument sensitivity to fast changes in wind signals, as occurs inside these events. In addition, the atmospheric dynamics at each landing site could be influencing the data. If so, Jezero crater, although with a similar number of pressure drops and intensity as observed at Elysium Planitia, would be subject to dramatic disturbances in the near-surface winds regarding the background winds by the passage of convective vortices, a much greater variation than at Elysium Planitia.

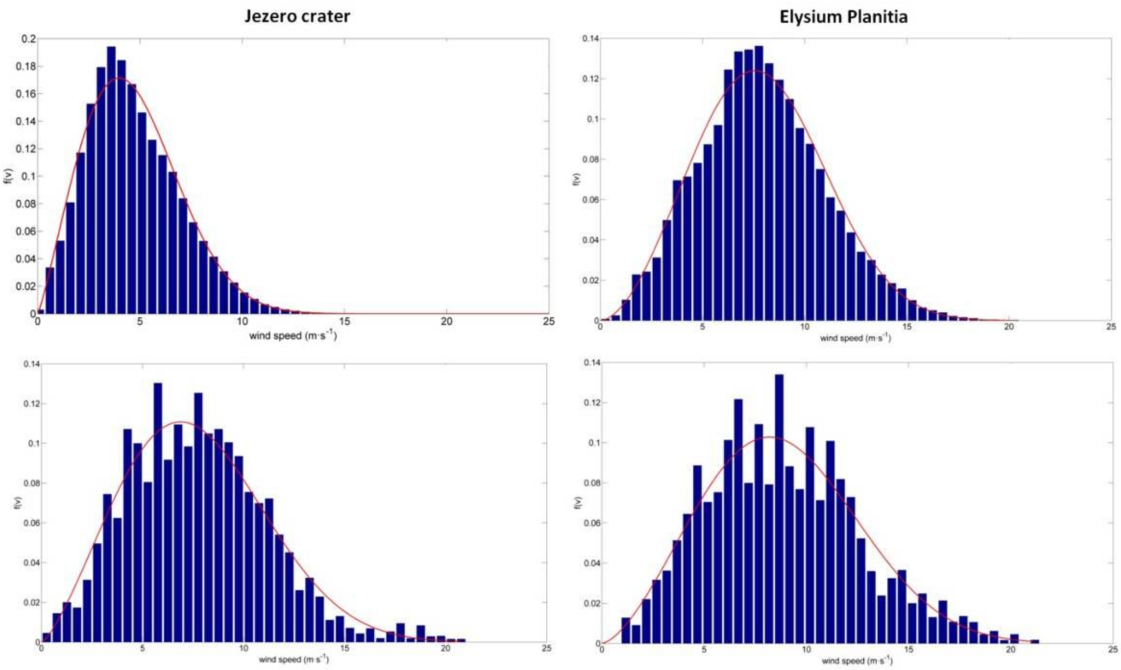

Fig. 9: Weibull probability density functions (PDFs) (red line) and comparison with empirical data (blue histogram) for the midday (MD timeslot), both for Jezero (left column) and Elysium Planitia (right column). (**top**) PDF for the whole MD timeslot period, (**bottom**) PDF of wind speeds in the MD timeslot but during pressure drop events (within ± 10 s around the events).

7. INTERACTION BETWEEN WINDS AND SURFACE

Sustained winds at Jezero were weak on average. Mean wind speeds were 3.2 ± 2.3 ms^{-1} in northern spring and summer, with a corresponding surface friction wind velocity, u_*, assuming a logarithmic profile, of 0.20 ms^{-1}. During the afternoon, winds were 6.1 ± 2.2 ms^{-1} ($u_* = 0.37$ ms^{-1}). The wind stress was generally less than 0.01 Pa even during daytime, when peak wind speeds were reached. However, strong aeolian activity has been observed at Perseverance's landing site.

The Jezero wind stress estimations differ from the estimated wind stresses in Elysium Planitia, ranging between 0.01 and 0.04 Pa, where rare aeolian changes were reported (Charalambous et al., 2021). The observed wind intensities and dust lifting events at Jezero suggest that sustained saltation is not responsible for the aeolian changes. However, although saltation due to aerodynamic shear at the fluid threshold is required to initiate grain motion, once started, there is no need for high wind speeds to maintain particle flux. On Mars, impact threshold speeds are only about 10% of the fluid threshold (Kok, 2010; Bridges et al., 2012). Thus, saltation may be initiated by high wind speeds reached eventually in short timescales, and moderate wind speeds would maintain significant fluxes of sand. This mechanism, proposed in previous missions to Mars (e.g., Bridges et al., 2012 and references therein), could be affecting, as well, the aeolian changes in Jezero (Newman et al., 2022). The dramatic disturbances in the near surface winds by the passage of convective vortices (Fig. 9), together with the turbulence levels and wave activity at Jezero, could be promoting aeolian activity (both dust lifting and sand motion) at Perseverance's landing site.

Although, to a large extent, the majority of the observed dust events were directly associated with the passage of convective vortices (i.e., dust devils) (e.g., Toledo et al., this issue), certain events can be associated with convection cell fronts for cases in which these fronts exceed the threshold wind speed (stress) required for dust lifting. Newman et al. (2022) presented one of these cases, observed on sol 117 by the Perseverance cameras and MEDA sensors. That distant dust-lifting event covered an estimated area of at least 4 km^2 and lasted several minutes, raising a dust cloud a couple of km to the north of the rover. We present in Fig. 10 another dust event, on sol 311 at 12.7 h LTST, which, unlike the previous one, passed over the rover. There are no images associated with this event, but wind speeds and directions and irradiance variations could be measured by the Radiative and Dust Sensor (RDS) of MEDA (Rodríguez-Manfredi et al., 2021; Apéstigue et al., 2022). The RDS includes channels in several spectral bands pointed at the zenith when the rover does not present tilt (*top* channels, referred hereafter as TN, where *N* is the specific number of the channel), in addition to 7 channels at 750 nm pointed at different azimuthal directions (*lat* channels, referred hereafter as LN, where *N* is the specific number of the channel), where L2 to L7 point at 70º zenith angle.

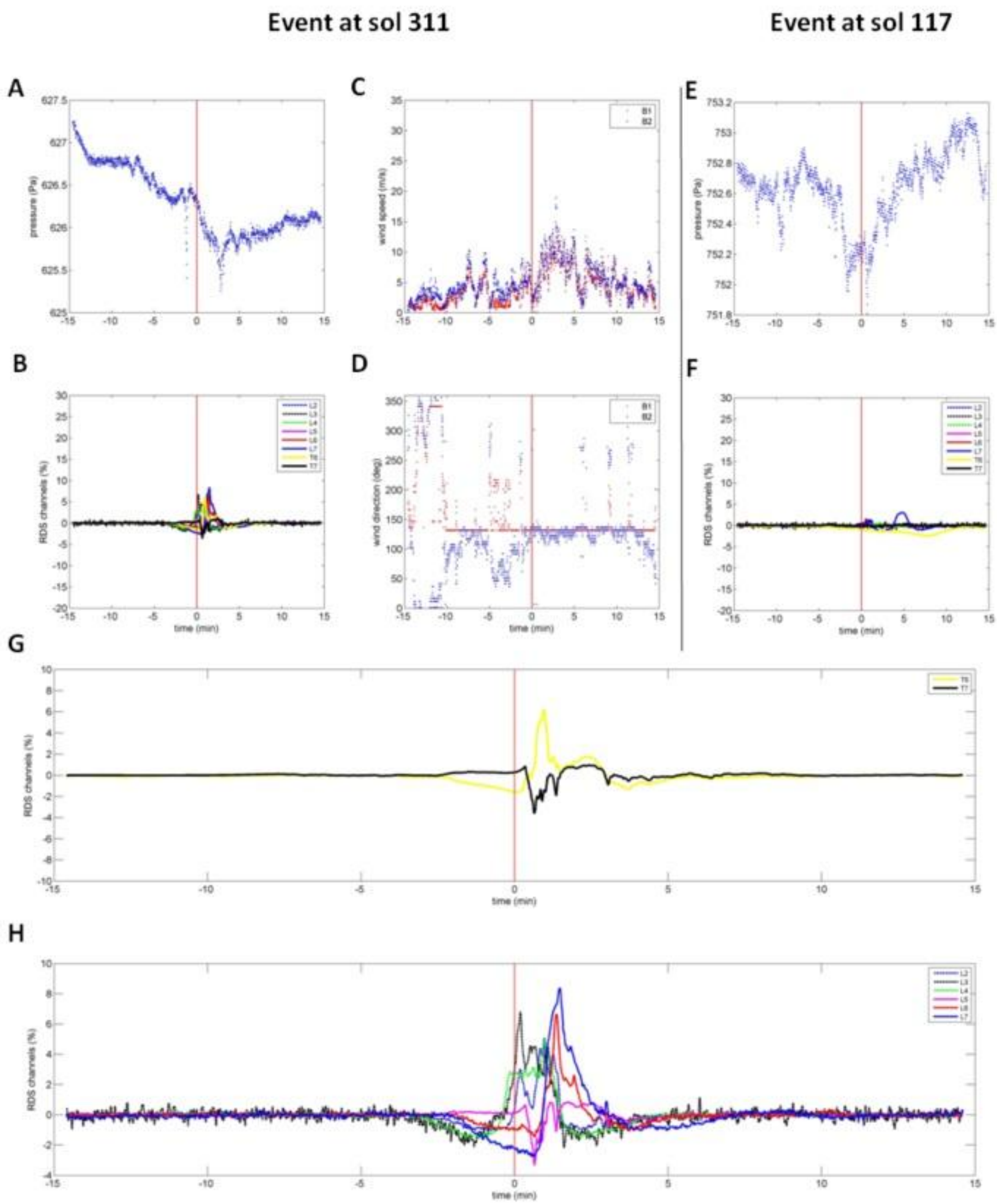

Fig. 10: Dust event at sol 311, 12.7 h LTST, not directly linked to convective vortex activity. ±15 min is shown around the event. Evolution in time of (**A**) pressure (Pa); (**B**) relative variation in RDS signals for both lateral and top channels; (**C**) wind speed (ms^{-1}) and (**D**) wind direction (deg). (**G and H**) enlargement of the RDS variations around the event, splitting between top and lateral RDS channels. (**E and F**) as in (A and B), but representing the event at sol 117 as reported in Newman et al. (2022) for comparison.

This dust event on sol 311 occurred between two major pressure drops separated by ~5 min, and in a context of large dust lifting and dust devil activity, preceding a regional dust storm. At the time of the event, pressure was falling and wind speed was rising, likely as a result of the passage of a convection cell advected by the background wind. Winds were west-southwesterly and roughly constant in this period, consistent with the upslope winds driving the daytime behavior. RDS variations began before the first pressure drop (Fig. 10A and 10B) in both the *lat* and the *top* channels (Fig. 10G and 10H). The disturbances were first observed in the L2, L3 and L4 channels (pointing to S, SE and E respectively). Then, the disturbances peaked in the *top* channels and disturbed the L5 channel (pointing to NE) and, finally, effects were observed in the L6 and L7 channels (pointing to N and NW). Variations greater than 8% were observed in some of the channels, including the *top* ones. The strong peak in T6 (>6%), which is sensitive to the scattered sunlight produced by the dust cloud in the close encounters, together with the variations in the remaining channels, indicate that the event passed over the rover. Overall, the event lasted around 10 min, with the core of the disturbances taking place in an interval lasting 3-4 min within two pressure drops, which were separated by ~5 min. Comparatively, the variations in irradiance during the event at sol 117, shown in Fig. 10 as well, peaked at ~3% in one lateral channel, and produced little or negligible effects in the remaining ones. The duration of the event and the measured winds together suggest that the dust cloud that passed over the rover may have been 0.5 - 1 km in length.

The dust lifting observed at Perseverance's landing site has also had major implications for instrumentation. The wind sensor suffered damage to some boards throughout the mission, probably due to flying debris. This issue was also reported for the MSL REMS wind sensor, which uses the same technology as the MEDA WS (Gómez-Elvira, 2014; Viúdez-Moreiras et al., 2019a; 2019b). On MSL REMS, the damage during MSL's landing on one sensor boom strongly limited the capability to derive winds. As the field of view for each sensor boom is constrained by the hardware and by the rover perturbations, both booms are necessary to properly measure winds independently of the incoming flow direction (see the companion paper, part 1); thus, it was necessary to develop new retrieval algorithms to characterize the wind patterns at Gale Crater (Viúdez-Moreiras et al., 2019a; 2019b). Later on, the remaining boom failed, probably by flying debris during intense wind periods as MSL climbed the slopes of Aeolis Mons, after successfully operating for ~1500 sols. The InSight wind sensor, using the same technology as well, has been successfully operating on Mars for more than 1000 sols, probably due to the lack of significant aeolian activity at that landing site.

A close encounter with a dust devil on sol 313 further damaged Perseverance's WS2. Fig. 11 presents the effect of the event at sol 313 on pressure, RDS channels and local winds as measured by Mars 2020. The wind retrieved for both sensor booms is presented as well. These signals are combined properly to derive the wind speed and direction (Gómez-Elvira et al., 2014; Viúdez-Moreiras et al., 2019a), promoting the sensor boom that is better oriented to the incoming wind direction. Here, it can be seen that before the encounter, WS2 was better oriented to the incoming flow while WS1 had a saturated signal. The encounter increased wind speeds, as usual during these events (Fig. 8 and Fig. 9), but in this case reaching extreme wind speeds greater than 20 ms^{-1}. Therefore, this event was one those producing the highest wind speeds recorded on Jezero.

The convective vortex also produced appreciable dust lifting (i.e., it was a dust devil), as the dramatic relative variations in the RDS irradiance signals indicated (greater than 10% variations both in RDS T6 and RDS T7 during the passage). Due to damage to a sensor board, probably by impacts with lifted dust in the electronics, WS2 stopped retrieving winds just when maximum wind speeds and signals of pressure drops were recorded. This loss prevented the current engineering retrieval from deriving wind magnitudes. The remaining boom, WS1, suffered a malfunction two sols later, on sol 315 and the wind sensor was turned off for several sols to analyze the issue.

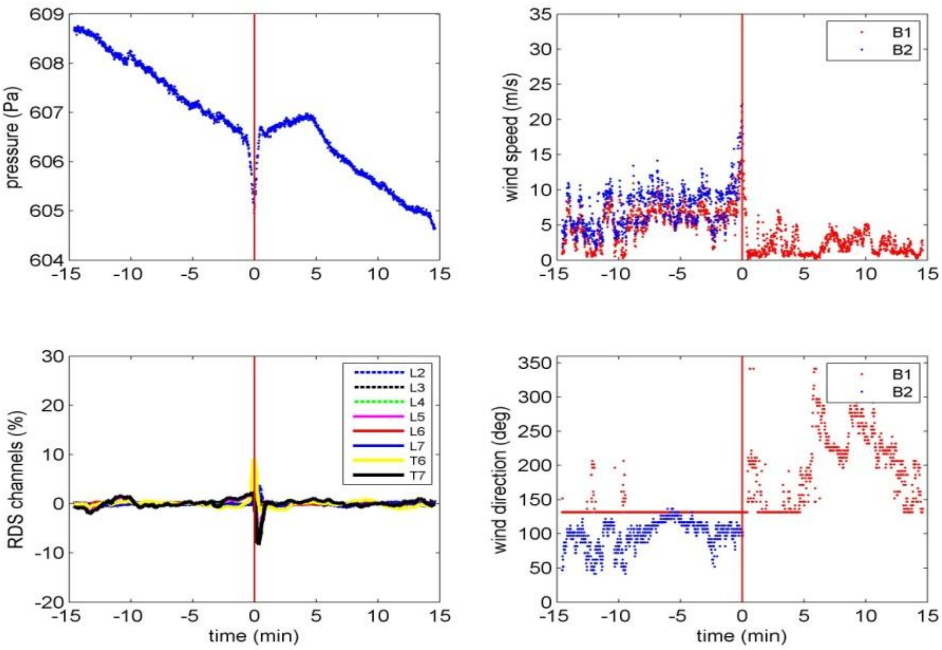

Fig. 11: Close encounter with a dust devil on sol 313 at 13:42 h LTST. ±15 min is shown around the maximum pressure drop. (**top-left**) pressure signal (Pa), (**top-right**) wind speed signal (ms^{-1}) for both WS1 and WS2, (**bottom-left**) relative variation in RDS signals for both lateral and top channels, (**bottom-right**) wind direction signal both for WS1 and WS2.

8. SUMMARY AND CONCLUSIONS

Sustained winds at Jezero as measured by Mars 2020 were weak on average. Mean wind speeds were 3.2 ± 2.3 ms^{-1} in northern spring and summer, with 99% of wind speeds below 10 ms^{-1}. During the afternoon, winds peaked and reached 6.1 ± 2.2 ms^{-1}. The wind stress was generally less than 0.01 Pa even during daytime, when peak wind speeds were reached.

The wind speeds were characterized by fitting the wind data as a Weibull distribution. InSight wind data acquired in Elysium Planitia were also used to contextualize the observations. The Weibull distribution fits the wind speed data at Jezero using a scale parameter c = 3.60 ms^{-1} and a shape parameter k = 1.49, and the wind data at Elysium Planitia using a scale parameter c = 6.20 ms^{-1} and a shape parameter k = 1.91. Elysium Planitia values align with those previously found for Gale crater, but Jezero winds strongly diverge and are much quieter than those found in previous missions. Among the three landing sites on Mars in which high-frequency measurements are available, Jezero crater shows the lowest wind speeds in the total winds. The probability of wind speeds greater than 12 ms^{-1} was 0.2% during the mission, and it was only close to 10% around the summer solstice afternoon. Wind speeds at Elysium Planitia were 68% greater, on average, than at Jezero. These results give quantitative indication that Perseverance landing site is less windy than InSight landing site, despite the intense aeolian activity observed at Jezero crater and the low aeolian activity reported at Elysium Planitia.

On the diurnal timescale, the wind speed distributions at Jezero, as well as at Elysium Planitia, presented a marked diurnal variation, in accordance with their changes in the wind regimes throughout the diurnal cycle, each landing site driven by its own mesoscale and large-scale phenomena. At the Jezero landing site, the highest average wind speeds were found during the afternoon and midday, presenting east-southeasterly and east-northeasterly (upslope) winds, with a marked difference from the remaining diurnal timeslots. From sunset to 01 h LTST, westerly/northwesterly downslope winds made wind speeds peak around midnight. After that, winds decreased towards a calm period lasting until sunrise. In Elysium Planitia, however, most of the diurnal timeslots showed both higher average wind speeds and steadiness than at Mars 2020 Perseverance's landing site at Jezero, the latter likely as a result of the lack of significant topography around InSight's landing site. The skewness of the distribution showed the opposite behavior in several diurnal timeslots at both landing sites. Additionally, the InSight and Mars 2020 data allowed studying of the sol-to-sol variability. On the seasonal timescale, the daytime diurnal timeslots, dominated by upslope winds, presented a seasonal behavior with maximum values in early summer. Conversely, the nighttime timeslots, dominated by downslope winds, presented a vast seasonal variability and roughly the opposite trend, with minimum values in early summer.

A great influence of turbulence, wave and vortex activity was observed in the wind speed variations, thus driving the highest wind speeds observed at Jezero, instead of sustained winds driven by mesoscale or large-scale dynamics. Mars 2020 MEDA wind data showed typical standard deviation of 0.57±0.29 ms^{-1} during nighttime and 1.85±0.57 ms^{-1} during the daytime in a ten-minute timescale, with peak values greater than ~3.5 ms^{-1} during the daytime.

The power spectral density of wind speed fluctuations follows a power-law, whose slope deviates depending on the time of day from that predicted considering homogeneous and isotropic turbulence, being higher at night, where the turbulence is mechanically driven. Turbulence and wave activity provoked rapid fluctuations that changed wind speed from calm conditions to more than 10 - 15 ms^{-1} on the timescale of seconds to minutes. These fluctuations dramatically disturbed the wind directions as well. Although the most intense fluctuations were observed during the daytime, nighttime fluctuations were also very high, suggesting strong mechanical turbulence during nighttime. The turbulence intensity levels detected by Mars 2020 at Jezero crater are greater than those detected by InSight at Elysium Planitia, and both produced by buoyancy and shear-driven turbulence.

We report periodic wind fluctuations that may be related to convection cells and smaller eddies in the PBL advected over the crater on different scales. The wave period varied by one order of magnitude, from the timescale of 1 min to 10 min, while background wind speeds were roughly similar. These periods would lead to length scales from a few hundred meters to 6 km, as indicative of the turbulent activity present on the daytime Martian PBL. The signature of convection cells was found during dust storm conditions, when winds are believed to be tidally driven instead of slope driven, complementing the detection of gravity waves after sunset as presented in part 1. It has been suggested that the Martian PBL depth could be inferred based on the estimated width of convection cells, which would provide valuable information about the PBL. However, these results suggest that is questionable to infer the PBL depth from estimations of wind fluctuations, which will likely not relate to the wider length scale of the convection cell, leading to significant underestimations of the PBL depth.

Pressure drops associated with convective vortices were usually involved in rapid wind fluctuations. Winds measured inside vortices showed relative variations between 0.8 and 9.2 times above the background winds. Weibull models were constructed in the periods around the pressure drops, detected throughout the mission, showing extreme winds around these events. The scale parameter c increased 65% and the shape parameter k kept roughly constant. This variation in the Weibull parameters resulted in a dramatic effect in the tail of the PDFs at Jezero, hence in the probability of high wind speeds. Thus, $P(v > 8\ ms^{-1})$ increased from 8.6% to 40% and $P(v > 12\ ms^{-1})$ further increased roughly 40 times inside the periods of these events. Curiously, the effect was not so pronounced in the InSight data. This difference between both missions was possibly affected by the reduced sensitivity to fast changes by the InSight wind sensor. Furthermore, the atmospheric dynamics at each landing site could be influential. If so, despite having a similar number of pressure drops and intensity to those observed at Elysium Planitia, Jezero crater would be subjected to dramatic disturbances in the near surface winds by the passage of convective vortices, with much greater variation than at Elysium Planitia.

We report the detection, by MEDA sensors, of a dust cloud on sol 311, associated with convective cell fronts passing over the rover. The duration of the event and the measured winds together suggest that the dust cloud that may have been 0.5 - 1 km in length. The variables measured by MEDA were strongly disturbed. The dust lifting events at Perseverance's landing site had major implications for the instrumentation. The wind sensor suffered damage to some boards throughout the mission probably due to flying debris. A close encounter with a dust devil on sol 313 further damaged the WS2, making the boom inoperative until new retrieval algorithms and calibration tests may allow for the use of the non-damaged boards of the sensor independently of the damage in the remaining parts.

DATA AVAILABILITY AND OPEN RESEARCH

The data used in this work are publicly available in the NASA's Planetary Data System (PDS) (https://pds.nasa.gov/).

AKNOWLEDMENTS

The authors acknowledge and thank the Mars 2020 team. This work is supported by the Spanish Ministry of Science and Innovation, under project RTI2018-098728-B-C31. Part of the research was carried out at the Jet Propulsion Laboratory, California Institute of Technology, under a contract with the National Aeronautics and Space Administration (80NM0018D0004). The UPV/EHU team is supported by Grant PID2019-109467GB-I00 funded by 1042 MCIN/AEI/10.13039/501100011033/ and by Grupos Gobierno Vasco IT1742-22.

REFERENCES

Apéstigue. et. al. (2022) Radiation and Dust Sensor for Mars Environmental Dynamic Analyzer Onboard M2020 Rover. *Sensors* 2022, 22, 2907. https://doi.org/10.3390/s22082907

Balme, M.R., A. Pathare, S.M. Metzger, M.C. Towner, S.R. Lewis, A. Spiga, L.K. Fenton, N.O. Rennó, H.M. Elliott, F.A. Saca, T.I. Michaels, P. Russell, J. Verdasca (2012) Field measurements of horizontal forward motion velocities of terrestrial dust devils: towards a proxy for ambient winds on Mars and earth, *Icarus*, 221 (2), 632-645,

Banfield, D., Spiga, A., et al. (2020) The atmosphere of Mars as observed by InSight. *Nat. Geosci*. 13, 190–198. https://doi.org/10.1038/s41561-020-0534-0

Basu, S., Wilson, R.J., Richardson, M.I., Ingersoll, A. (2006) Simulation of spontaneous and variable global dust storms with the GFDL Mars GCM. *J. Geophys. Res*. 111, E09004

Bridges, N., Ayoub, F., Avouac, JP. et al. (2012) Earth-like sand fluxes on Mars. *Nature* 485, 339–342. https://doi.org/10.1038/nature11022

Charalambous, C., et al. (2021) Vortex-dominated aeolian activity at InSight's landing site, Part 1: Multi-instrument observations, analysis and implications. *J. Geophys. Res*. 126, e2020JE006757 doi: 10.1029/2020JE006757

Comola, F., Kok, J. F., Chamecki, M., & Martin, R. L. (2019). The intermittency of wind-driven sand transport. *Geophysical Research Letters*, 46, 13,430–13,440. https://doi. org/10.1029/2019GL085739

Etiope, G., & Oehler, D. Z. (2019). Methane spikes, background seasonality and non-detections on Mars: A geological perspective. *Planetary and Space Science*, 168, 52– 61.

Forget, F., Banfield, D., Millour, E., Spiga, A., Newman, C., Viúdez-Moreiras, D., Pla-Garcia, J., Navarro, S., Mora-Sotomayor, L., Torres-Redondo, J., Rodriguez-Manfredi, J. A., Lewis, S., Lorenz, R., Lognonne, P., & Banerdt, B. (2019). Mars large scale meteorology observed by InSight. Paper presented at EPSC-DPS Joint Meeting 2019, EPSC-DPS2019–903.

Gomez-Elvira, J., Armiens, C., Castaner, L., Dominguez, M., Genzer, M., Gomez, F., Haberle, R., Harri, A.M., Jimenez, V., Kahanpaa, H., Kowalski, L., (2012). REMS: the environmental sensor suite for the Mars Science Laboratory rover. *Space Sci. Rev*. 170 (1-4), 583–640.

Haberle, R. M. et al. (1993) Mars atmospheric dynamics as simulated by the NASA Ames General Circulation Model: 1. The zonal-mean circulation. *J. Geophys. Res*. 98, 3093–3123.

Hess, S.L., Henry, R.M., Leovy, C.B., Ryan, J.A., Tillman, J.E., (1977). Meteorological results from the surface of Mars: Viking 1 and 2. *J. Geophys. Res*. 82 (28), 4559–4574.

Holstein-Rathlou, C., et al. (2010), Winds at the Phoenix landing site, *J. Geophys. Res*., doi:10.1029/2009JE003411

Hueso, R., et al. (2022) Convective vortices and dust devils detected by Mars 2020, *JGR-Planets*, this issue.

Kahanpää, H. & Viúdez-Moreiras, D. (2021). Modelling martian dust devils using in-situ wind, pressure, and UV radiation measurements by Mars Science Laboratory. *Icarus*, 359, 114207. https://doi.org/10.1016/j.icarus.2020.114207

Kahre, M.A., Murphy, J.R., Haberle, R.M. (2006) Modeling the martian dust cycle and surface dust reservoirs with the NASA Ames general circulation model. *J. Geophys. Res*. 111, E06008

Kahre, M. A. et al. (2017) The Mars dust cycle. Atmos. Clim. Mars 18, 295.

Kok, J. F. (2010). An improved parameterization of wind-blown sand flux on Mars that includes the effect of hysteresis. *Geophysical Research Letters*, 37, L12202. https://doi.org/10.1029/2010GL043646

Kok et al (2012) *Rep. Prog. Phys*. 75 106901

Lemmon M.T., M.D. Smith, D. Viudez-Moreiras, M. de la Torre-Juarez, A. Vicente-Retortillo, A. Munguira, A. Sanchez-Lavega, R. Hueso, G. Martinez, B. Chide, R. Sullivan, D. Toledo, L. Tamppari, T. Bertrand, J.F. Bell III, C. Newman, M. Baker, D. Banfield, J.A. Rodriguez-Manfredi, J.N. Maki, V. Apestigue (2022) Dust, Sand, and Winds within an Active Martian Storm in Jezero Crater, *Geophys. Res. Lett.* (under review)

Lorenz, R.D., (1996). Martian surface wind speeds, described by the Weibull distribution. *J. Spacecraft Rockets* 33, 754–756.

Lorenz, R.D., Nakamura, Y., & Murphy, J. R. (2017) Viking-2 seismometer measurements on Mars: PDS data archive and meteorological applications. *Earth and Space Science*, 4, 681–688.

Lorenz, R.D., Lemmon, M.T. & Maki, J. (2021) First Mars year of observations with the InSight solar arrays: Winds, dust devil shadows, and dust accumulation. *Icarus*, 364, 114468.

Mason, E.L. & Smith, M.D. (2021) Temperature fluctuations and boundary layer turbulence as seen by Mars Exploration Rovers Miniature Thermal Emission Spectrometer, 360, 114350

Murdoch et al. (2017) Evaluating the wind-induced mechanical noise on the InSight seismometers. *Space Sci Rev*, 211, 429-455.

Newman, C.E. et. al. (2022) The dynamic atmospheric and aeolian environment of Jezero Crater; Mars, *Science Advances*, 8(21), eabn3783.

Petrosyan, A., Galperin, B., Larsen, S. E., Lewis, S. R., Maattanen, A., Read, P. L., et al. (2011). The Martian atmospheric boundary layer. *Reviews of Geophysics*, 49, 3005

Pollack, J. B., Colburn, D. S., Flasar, F. M., Kahn, R., Carlston, C. E., and Pidek, D. (1979), Properties and effects of dust particles suspended in the Martian atmosphere, J. Geophys. Res., 84(B6), 2929– 2945, doi:10.1029/JB084iB06p02929.

Roback et al. (2022) Multi-year measurements of ripple and dune migration on Mars: Implications for the wind regime and sand transport. *Icarus*, 380, 114966

Rodríguez-Manfredi et al., (2021) The Mars Environmental Dynamics Analyzer, MEDA. A Suite of Environmental Sensors for the Mars 2020 Mission. *Space Science Reviews*, 217:48

Sánchez-Lavega, A., del Río-Gaztelurrutia, T., Hernández-Bernal, J., & Delcroix, M. (2019). The onset and growth of the 2018 Martian Global Dust Storm. *Geophysical Research Letters*, 46, 6101–6108.

Seguro, J.V. & Lambert, T.W. (2000) Modern estimation of the parameters of the Weibull wind speed distribution for wind energy analysis, Journal of Wind Engineering and Industrial Aerodynamics, 85(1), 75-84.

Spiga, A. & Forget, F. (2009) A new model to simulate the Martian mesoscale and microscale atmospheric circulation: validation and first results. *J Geophys Res Planets* 114:E02009

Spiga, A., Murdoch, N., Lorenz, R., Forget, F., Newman, C., Rodriguez, S., et al. (2021). A study of daytime convective vortices and turbulence in the Martian planetary boundary layer based on half-a-year of InSight atmospheric measurements and large-eddy simulations. *Journal of Geophysical Research: Planets*, 126, e2020JE006511.

Stull, R. B. (2012). An introduction to boundary layer meteorology (Vol. 13). Heidelberg: Springer Science & Business Media.

Sullivan et al. (2020). A Broad Continuum of Aeolian Impact Ripple Morphologies on Mars is Enabled by Low Wind Dynamic Pressures, Journal of Geophysical Research: Planets, 125(10),e2020JE006485

Viúdez-Moreiras, D., Gómez-Elvira, J., Newman, C.E, Navarro, S., Marin, M., Torres, J., de la Torre, M. & the MSL team. (2019a) Gale Surface Wind Characterization based on the Mars Science Laboratory REMS Dataset. Part I: Wind Retrieval and Gale's Wind Speeds and Directions. *Icarus*, 319, 909-925.

Viúdez-Moreiras, D., Gómez-Elvira, J., Newman, C.E, Navarro, S., Marin, M., Torres, J., de la Torre, M. & the MSL team (2019b) Gale Surface Wind Characterization based on the Mars Science Laboratory REMS Dataset. Part II: Wind Probability Distributions. *Icarus*, 319, 645-656.

Viúdez-Moreiras, D., Newman, C.E., Forget, F., Lemmon, M., Banfield, D., Spiga, A., Lepinette, A., Rodriguez-Manfredi, J.A., Gomez-Elvira, J., Pla-Garcia, J., Muller, N., Grott., M. & the TWINS/InSight team (2020c). Effects of a large dust storm in the near-surface atmosphere as measured by InSight in Elysium Planitia, Mars. Comparison with contemporaneous measurements by Mars Science Laboratory. *JGR: Planets*, 125, e2020JE006493. https://doi.org/10.1029/2020JE006493

Viúdez-Moreiras, D. (2021b) A Three-Dimensional Atmospheric Dispersion Model for Mars. *Progress in Earth and Planetary Science*, 8(53). https://doi.org/10.1186/s40645-021-00445-4.

Wang, H., Richardson, M.I., Wilson, R.J., Ingersoll, A.P., Toigo, A.D. (2003) Cyclones, tides, and the origin of cross-equatorial dust storms on Mars. *Geophys. Res. Lett*. 30, 1488.

Wang, H., Zurek, R.W., Richardson, M.I. (2005) Relationship between frontal dust storms and transient eddy activity in the northern hemisphere of Mars as observed by Mars Global Surveyor. *J. Geophys. Res*. 110, E07005.

Wilson, R. J. & Hamilton, K. (1996) Comprehensive model simulation of thermal tides in the Martian atmosphere. *J. Atmos. Sci*. 53, 1290–1326.